Synthesis, characterization and anticancer activities of cationic η^6-*p*-cymene ruthenium(II) complexes containing phosphine and nitrogenous ligands

Ivelise Dimbarre Lao Guimarães,[a] Flávia Marszaukowski,[a] Priscila Buhrer Rutka,[a] Luis Felipe Borge,[a] Renan Augusto Pontes Ribeiro,[b] Sergio Ricardo de Lazaro,[a] Patrícia Castellen,[c] Araba Sagoe-Wagner, [d] Roy M. Golsteyn,[d] René T. Boeré*[e] and Karen Wohnrath*[a]

[a] Departamento de Química, Universidade Estadual de Ponta Grossa, Av. Gal. Carlos Cavalcanti, 4748, Uvaranas, CEP 84030-900, Ponta Grossa, PR, Brasil.
[b] Departamento de Química, Universidade do Estado de Minas Gerais, Av. Paraná, 3001, Jardim Belvedere, CEP 35501-170, Divinópolis, MG, Brasil.
[c] Instituto Federal Catarinense, Rua das Rosas, s/n, Vila Nova, CEP: 88965-000, Santa Rosa do Sul, SC, Brasil.
[d] Department of Biological Sciences, University of Lethbridge, 4401 University Drive, Lethbridge, Alberta, Canada T1K 3M4.
[e] Department of Chemistry and Biochemistry, University of Lethbridge, 4401 University Drive, Lethbridge, Alberta, Canada T1K 3M4.

ABSTRACT

Ruthenium-based anticancer agents have created a center of attention in the field of inorganic medicinal chemistry. The first fully characterized cationic ruthenium(II)-arene complexes [Ru(η^6-*p*-cymene) (PAr_3)$L^NCl]^+$ with highly lipophilic PAr_3 ligands where Ar = 3,5-$((CH_3)_3C)_2C_6H_3$– (**L1**), 3,5-$(CH_3)_2C_6H_3$– (**L2**), 4-CH_3O-3,5-$(CH_3)_2C_6H_2$– (**L3**) and 4-CH_3O-C_6H_4– (**L4**) with N = 3-methylpyridine (**1-4**, respectively), or **L4** and 4-methylpyridine (**5**), or **L4** and CH_3CN (**6**) were obtained (yields 67-91%) as solids stable to light and air. Electrical conductance indicates that all the complexes are 1:1 electrolytes in solution. Their composition and purity have been unambiguously established by single-crystal X-ray diffraction, NMR spectroscopy and elemental analysis. The coordination geometries are uniform for all six complexes and each structure consist of a unipositive complex cation bearing the phosphine ligands **L1**-**L4** and L^N = 3-methylpyridine, 4-methylpyridine or CH_3CN attached to the organometallic fragment. The equivalent unit cell

volumes per formula unit decrease with **1** > **3** > **2** > **4** > **5** > **6**, accurately reflecting the decreasing sizes of the phosphines **L1**-**L4**, and a greater occupied volume for 3-methyl- vs. 4-methylpyridine, and the smallest volume contribution from CH_3CN. Electrochemical studies showed mixed electrochemical mechanisms (EC/ECE) from partial substitution of *p*-cymene by CH_3CN ligands from the solvent. A large electrochemical stability window (>2.2 V) for Ru(II) was observed extending beyond the physiological E° range. The complexes were cytotoxic against human cancer cell lines *in vitro*, and some complexes altered cell morphology.

Keywords*:* Cationic ruthenium-arene. Triarylphosphine. Pyridine derivative. Cyclic voltammetry. Cytotoxicity assays. DFT calculations.

Introduction

Despite advances in the treatment of cancer, cisplatin and its derivatives are still used in chemotherapy treatment [1], despite that these drugs have limitations such as the lack of specificity that results in numerous undesirable side effects [2] and post-treatment drug resistance [3]. Thus, the search for new metallodrugs to overcome these limitations has increasing impetus [4]. Complexes containing ruthenium as a metallic center have been explored as possible metallopharmaceuticals, and some synthesized complexes, such as NKP1339, NAMI-A, RM175 and RAPTA-C have been in clinical trials, which serve as inspiration for current research [5-7].

A variety of organometallic ruthenium(II) complexes containing arene ligand coordinated in η^6 form are being investigated for their properties, such as versatility in ligand exchange, ease of complexation reactions [8-10], ability to stabilize the oxidation state of ruthenium 2+ under physiological conditions [11-13] and providing a hydrophobic surface that facilitates the transport across the plasma membrane [14,15]. Phosphine ligands are widely used in coordination chemistry, since they have both electron donor and acceptor capacities, which helps to stabilize both higher and lower transition metal valences [16-18]. Regarding complexes with triarylphosphine ligands and their derivatives, Sáez and co-workers reported a neutral ruthenium(II) arene complex [Ru(η^6-*p*-cymene)(PPh_3)Cl_2] (PPh_3 = triphenylphosphine) used as precursor of a series of cationic complexes [19]. Arene ruthenium cationic complexes containing nitrogenous ligands have attracted attention due to their photochemical, electrochemical and biological applications, which

are more cytotoxic than cisplatin [20-24]. Solvent-coordinated transition metal complexes, such as acetonitrile, have been synthetized since the solvato ligands are usually labile, making them versatile reagents [25]. After the discovery that RDC11 (a cationic organometallic Ru(II)-CH_3CN complex) reduces tumor growth in different mouse models [26], some cationic Ru(II)-CH_3CN compounds with potent cytotoxic activities have been described, for example [Ru(η^6-*p*-cymene)L($NCCH_3$)]$^+$ (where L are 2-phenylindole derivatives) [27]; κ^1-P-[Ru(η^6-*p*-cymene)($NCCH_3$)(1,4,7-triaza-9-phosphatricyclo[5.3.2.1]tridecane)Cl]PF_6 [28]; [Ru(η^6-*p*-cymene)($NCCH_3$)(L)Cl]PF_6 (where L is 2-(4-nitrophenyl)imidazo[1,5-a]pyridin-2-ylidene) [29].

Several studies have shown that cytotoxicity and cancer cell selectivity depend on the choice of phosphine [19,28,30-33]. As part of our efforts to develop new drugs with reduced toxicity and side-effects, [Ru(η^6-*p*-cymene)(PAr_3)Cl_2] (Ar = 3,5-$((CH_3)_3C)_2C_6H_3$ (**L1**), 3,5-$(CH_3)_2C_6H_3$ (**L2**), 4-C_6H_3O-3,5-$(CH_3)_2C_6H_2$ (**L3**) and 4-CH_3O-C_6H_4 (**L4**)) were synthetized in our group (i.e. the precursor complexes **P1 – P4** in Chart 1) [34]. The antitumor results obtained for this series indicate that all the complexes were active against tumor cells (MDA-MB-231 and A549), with **P1** considered the most promising, since it was not cytotoxic against the healthy cells. The performance of these complexes was found to be dependent of the structural geometry of PAr_3 ligands [34].

These phosphines, which display strong donor properties and high lipophilicity with varying degrees of distal steric bulk [35], had their basicity well established by voltammetry and DFT computation [35]. The basicity for the phosphines $P(Ph)_{3-n}\{4\text{-}RO\text{-}3,5\text{-}(^tBu)_2\text{-}C_6H_2\}_n$ (n = 1, 3; R = $SiMe_3$, H) with n = 3, R = H was also determined using the $^1J_{P,Se}$ values of the respective selenides. The results indicate that the described phosphine is the most basic triarylphosphine ever reported [36]. As strong donors, the expectation is that the Ru-phosphine bonds will be very robust, protecting the active agents in medicinal applications.

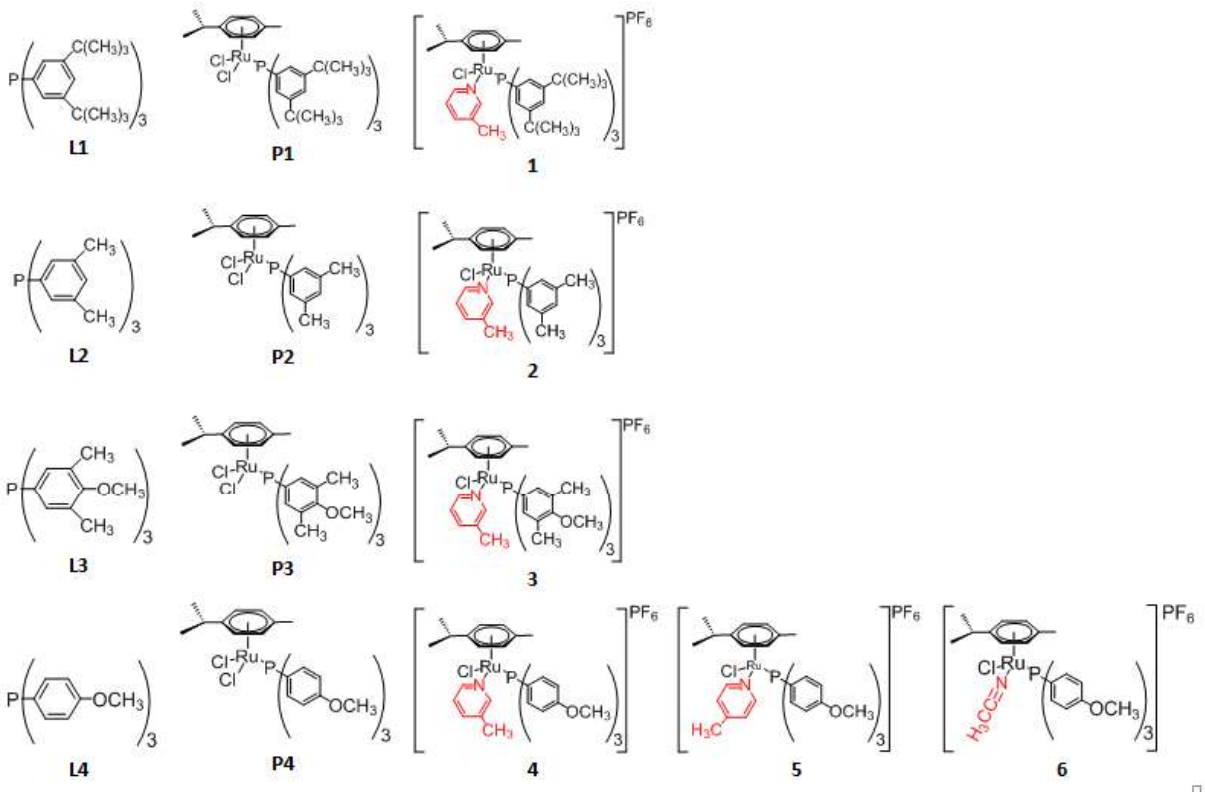

Chart 1. Structures of the ligands (**L1**-**L4**), precursors (**P1**-**P4**) and cationic complexes (**1**-**6**) in this work.

Here we report on new complexes **1 – 6** by exchanging of one of the chloro ligands by nitrogen-donor ligands L^N, giving rise to a series of cationic complexes with the general formula $[Ru(\eta^6\text{-}p\text{-cymene})(PAr_3)L^NCl][PF_6]$, where PAr_3 = **L1-L4** and L^N = 3-methylpyridine, 4-methylpyridine or acetonitrile (Chart 1). All the new complexes are fully characterized including single-crystal X-ray diffraction (SC-XRD) structures. Their redox behaviour has been thoroughly examined by solution-phase cyclic voltammetry (CV). These complexes demonstrate a cytotoxic effect for U2OS (bone cancer) and HT-29 (colon cancer) cell lines. The cell morphology was affected by the complexes, which was consistent with vesicle formation, suggesting that the mechanism of action might be different from that of cisplatin.

Experimental section

Materials and general methods

The triarylphosphine ligands **L2**, **L3** and **L4** were obtained from Sigma-Aldrich as well as the ligands 3-methylpyridine and 4-methylpyridine. The ligand **L1** and the precursor complexes [Ru(η^6-*p*-cymene)(PAr_3)Cl_2] were prepared according to published procedures [34]. Silver hexafluorophosphate ($AgPF_6$), potassium hexafluorophosphate (KPF_6) and tetrabutylammonium perchlorate (TBAP, $C_{16}H_{36}ClNO_4$) are commercial products (Sigma-Aldrich) and used as received. The solvents were rigorously purified by standard procedures [37].

Physical measurements

FT-IR spectra (4000-550 cm^{-1}) were recorded on a DRS-8000/Shimadzu IRPrestige-21 spectrometer. UV-vis spectra (0.1 mmol) were recorded on a Varian Cary 50 Bio spectrophotometer using quartz cells, in the range 200-900 nm. Conductivity values were obtained using an Infolab WTW TetraCon® 325 conductivity bridge in a thermostated bath held at 25.0 °C. $1 \cdot 10^{-3}$ $mol \cdot L^{-1}$ [^{n}Bu_4N][ClO_4] solutions were used as the 1:1 electrolyte standard in CH_3CN, for which the molar conductance is 160.1 S cm^2 mol^{-1} [38]. 1D (^1H, $^{13}C\{^1H\}$, $^{31}P\{^1H\}$) and 2D (^1H–^1H gCOSY,^1H–^{13}C gHSQC, and ^1H–^{13}C gHMBC) solution-phase NMR experiments were recorded on a Bruker Avance III 700 MHz spectrometer, at probe temperature using, in general, 20 mg samples of complexes dissolved in $CDCl_3$, containing a trace amount of tretramethylsilane (TMS) that was used as an internal reference (0 ppm). Archival spectral data is presented in the SI. Cyclic voltammetry (CV) was carried out in dry CH_3CN with tetrabutylammonium perchlorate (TBAP Sigma-Aldrich) in $1.0 \cdot 10^{-3}$ $mol \cdot L^{-1}$ as a supporting electrolyte at room temperature (~25 °C) under a nitrogen atmosphere using a μ-Autolab (Type III, Metrohm-Eco Chemie) potentiostat/galvanostat connected to a computer controlled by GPES 4.9 (General Purpose Electrochemical System) software. The electrochemical cell was equipped with a glassy carbon (A = 3 mm^2) working electrode, a platinum foil auxiliary electrode and Ag/AgCl as the reference electrode in a Luggin capillary probe. Under these conditions, the ferrocenium/ferrocene redox couple was used as an internal reference ($E_{1/2}$ = 0.46 V *vs* Ag/AgCl). Elemental analyses were performed on Fisons CHNS, mod. EA 1108 elemental analyzer.

Computational methodology

Ab-initio calculations were carried out in vacuum at zero Kelvin for three representative models described as $[Ru(\eta^6\text{-}p\text{-cymene})(PPh_3)L^NCl]^+$ with L^N = 3-methylpyridine (describing the complexes **1**-**4**); 4-methylpyridine (**5**); and acetonitrile (**6**). Computational simulations based on Density Functional Theory (DFT) combined with the hybrid functional B3LYP [39,40], both employed in the GAUSSIAN09 [41] program were considered, where the C, H, Cl, and N atoms were represented by all-electron 6-31G+(d) basis set; while the Sapporo base set (SPK-DZCD) was employed for the Ru atoms. To optimize the molecular geometries, SCF calculations based on the Hartree-Fock formalism were undertaken and the total energy criteria was defined as 10^{-6} Hartree and 10^{-8} Hartree, respectively. The UV-Vis experiments were drawn from Frontier Molecular Orbital (FMOs) contributions, as they can locate electron densities where there is a possibility of electronic excitation, associated with the theoretical UV-Vis spectra obtained within Time-Dependent Density Functional Theory (TD-DFT). The FMO atomic orbital contributions were analyzed using Multiwfn [42]. To assist with elucidating the voltammetric results, the molecular geometries were also investigated as a function of the addition/removing of electrons based on resulting structural (bond distance and angle) and electronic parameter (FMOs energy) changes.

Cell culture and Cytotoxicity assays

Cytotoxicity tests of **1**-**6** were evaluated against two cell lines, U2-OS and HT-29. The human bone osteosarcoma cell line U2-OS (ATCC HTB-96) was cultured in Dulbecco's Modified Eagle's Medium ((DMEM)/F-12 (Gibco; 11320-082)) culture medium, containing 10% fetal bovine serum (FBS) (Gibco; 12484028), 2 mM Medium Eagle Medium non-essential amino acids (MEM NEAA) (Gibco; 11140050) and 15 mM HEPES (4-(2-hydroxyethyl)-1-piperazineethanesulfonic acid), pH 7.4. The HT-29 human colorectal adenocarcinoma cell line (ATCC HTB-38) was maintained in RPMI 1640 medium (Gibco; 21870-092) supplemented with 10% (v/v) FBS and 1.6 mM GlutaMAX (Gibco; 35050-061). Cells were grown at 37°C in 5% CO_2 and media were changed every two to three days. Cells were plated at $5.0x10^5$ cells/75 cm^2 flask and cultured for 48 h before treatment. Cisplatin complex (Calbiochem 232120; 300 g/mol) was prepared in DMSO at a concentration of 25 mM and stored for a maximum of 2 weeks at -20°C.

Cells were seeded at $1.0.10^5$/well in a 6-well culture plate and incubated at 37°C for 48 h before treatment. These cells were treated with DMSO (0.1% volume/volume) as a control solvent, with cisplatin at 25 µmol L^{-1} or with the complexes in a range of concentrations (0.5, 1.0, 1.5 µmol L^{-1}). Live cell images were captured at room temperature with an Infinity 1 camera operated by Infinity Capture imaging software (Lumenera Corporation) on an Olympus CKX41 inverted microscope. Images were processed using Adobe Photoshop (CC 2015.0.0).

The cytotoxicity of test chemicals **1**-**6** on U2OS and HT-29 cells was measured by the micro-culture tetrazolium assay (MTT; (3-(4,5)-dimethylthiazol-2-yl)-2,5-diphenyl-tetrazolium bromide (Sigma-Aldrich; M2128-1G)). Cells were plated at 3.8 x 10^5 cells/96 well culture plate and cultured at 37°C for 24 h prior to treatment. All measurements were performed in triplicate at 96 h and experiments were performed three times. After the specified treatment time, MTT solution (5 mg/ml MTT in phosphate buffered saline (PBS) (137 mM NaCl, 3 mM KCl, 100 mM Na_2HPO_4, 18 mM KH_2PO_4) was added to the media in each well. The media were then aspirated and MTT solvent (4 mM HCl, 0.1% (v/v) IPEGAL (octylphenoxypolyethoxyethanol), in isopropanol) was added to each well. Plates were shaken, and absorbance was measured at 590 nm using a BioTek microplate spectrophotometer powered by Eon software. Results were expressed as IC_{50} concentrations; the concentration of the compound that reduced the absorbance of MTT by 50%, by comparison to 0.1% (v/v) DMSO treated cells. The normalized percent absorbance was calculated as shown:

$$\text{Normalized percent absorbance} = (\text{absorbance}/\text{DMSO absorbance}) \times 100$$

The log concentrations of the compound were plotted against the normalized percent absorbance using Microsoft Excel software. Analysis was performed with GraphPad Prism 5 software, using non-linear regression (log(inhibitor) versus normalized response), to estimate the IC_{50} concentrations. Standard curves were plotted using the equation:

$$Y = \text{maximum} + (\text{maximum} - \text{minimum})/(1+10^{(x-\text{Log}IC_{50})})$$

Where maximum is the percentage of viable cells after treatment with 0.1% DMSO, minimum is the percentage of viable cells after treatment with the highest concentration of the genotoxic molecule and x is the log10 value of the treatment concentration.

*General procedure for synthesis of complexes (**1-6**)*

The syntheses of the 3- and 4-methylpyridine complexes used a route adapted from the literature [19], with agitation of the solution of the precursor complexes **P1 – P4** with the ligand 3-methylpyridine (**1-4**) and 4-methylpyridine (**5**) and with KPF_6 salt in the ratio 1:1:1 (**1**, **2**, **4**, **5**) and in the ratio 1:2:1 (**3**) in degassed CH_3OH (5 mL) for 4 h at room temperature. The solid precipitated was filtered off, washed with chloroform and diethyl ether, filtered off, and dried under reduced pressure. The synthesis of complex (**6**) was carried out from **P4** and $AgPF_6$ salt in a 1:1 ratio in acetonitrile; this mixture was stirred and heated under reflux for a period of 4 hours. The precipitated solid was filtered off, washed with diethyl ether, filtered off, and dried under reduced pressure. A bulk crystallization was undertaken in order to obtain purified compounds for all the characterizations and biological tests. The crystallization steps were performed in r.t. as following: for **1** crystals were grown by slow evaporation in diethyl ether; crystals for **2-4** were grown from a saturated solution of chloroform with slow infusion of diethyl ether and crystals for **5** and **6** were grown by slow infusion of diethyl ether in dichloromethane.

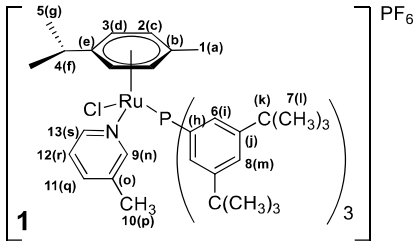

[Ru(η^6-*p*-cymene){P(C$_6$H$_3$-3,5-^{t}Bu$_2$)$_3$}(NC$_5$H$_4$-3-Me)Cl]PF$_6$ (**1**). Orange solid. Yield: 40.4 mg (72.70 %). MM: 1107.47 g·mol^{-1}. M.p.: 150–160 °C (dec) Elemental analysis calc. for: $C_{58}H_{84}ClF_6NP_2Ru$ (%): C, 62.89; H, 7.64; N, 1.26. Found: C, 61.37; H, 6.95; N, 1.30. Λm: 126.1 S cm^2 mol^{-1} (24 h, 25ºC). $^{31}P\{^1H\}$ NMR (161.97 MHz, $CDCl_3$, δ ppm): 39.92; -131 to -157 (sept, PF_6). ^1H NMR (700 MHz, $CDCl_3$, δ ppm): H_5 1.13 (dd, 6H, J_{H-H} = 9.80 Hz); H_7 1.18 (s, 54H); H_1 1.56 (s, 3H); H_{10} 2.14 (s, 3H); H_4 2.28 (sept, 1H, J_{H-H} = 13.59 Hz); H_2 5.16 (d, 1H, J_{H-H} = 5.95 Hz);

$H_{2'}$ 5.40 (d, 1H, J_{H-H} = 5.88 Hz); H_3 5.83 (d, 1H, J_{H-H} = 5.88 Hz); $H_{3'}$ 5.88 (d, 1H, J_{H-H} = 5.81 Hz); H_{12} 7.04 (t, 1H, J_{H-H} = 6.23 Hz); H_6 7.09 (s, 6H); H_{11} 7.42 (d, 1H, J_{H-H} = 7.49 Hz); H_8 7.48 (s, 3H); H_9 8.55 (s, 1H); H_{13} 8.61 (d, 1H, J_{H-H} = 4.76 Hz).$^{13}C\{^1H\}$ NMR (176.12 MHz, $CDCl_3$, δ ppm): C_a 17.45; C_g 18.32; C_k 21.07; C_p 22.97; C_f 30.57; C_l 35.00; $C_{c'}$ 84.86 (d, J_{C-H} = 7.12 Hz); C_c 87.97; C_d 90.20; $C_{d'}$ 92.59; C_b 102.95; C_e 114.62 (d, J_{C-H} = 6.53 Hz); C_r 125.17; C_i 128.28; C_j 135.84; C_m 139.09; C_q 139.19; C_o 150.88; C_s 153.11; C_n 156.72.C, H assign confirmed by COSY, HSQC, HMBC (see S.I.) (FTIR, cm^{-1}): 3072 (ν_{asCsp^2-H}), 2964, 2907, 2868 (ν_{asCsp^3-H}), 1473, 1420 ($\nu_{asC=C}$), 1586 ($\nu_{asC=N}$), 1127, 557 (ν_{P-C}), 847 ν_{PF6^-}, 705 (δ_{C-H}(aromatic ring)). UV-vis (CH_2Cl_2, 1 x 10^{-4} mol L^{-1}) λ max/nm (ε max/L mol^{-1} cm^{-1}): 243 (13340); 276 (7500); 336 (1690); 548 (780).

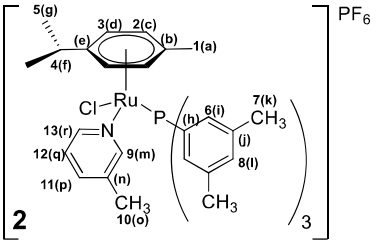

[Ru(η^6-*p*-cymene){P(C$_6$H$_3$-3,5-(Me)$_2$)$_3$}(NC$_5$H$_4$-3-Me)Cl]PF$_6$ (2). Orange solid. Yield: 39.2 mg (67.90 %). MM: 973.10 g·mol^{-1}. M.p.: 145–167 °C (dec). Elemental analysis calc. for: $C_{40}H_{48}ClF_6NP_2Ru{\cdot}0.5CHCl_3$ (%): C, 53.16; H, 5.34; N, 1.53. Found: C, 53.08; H, 5.20; N, 1.47. Λm: 127.5 S cm^2 mol^{-1} (24 h). $^{31}P\{^1H\}$ NMR (161.97 MHz, $CDCl_3$, δ ppm): 35.86; -131 to -157 (sept, PF_6). ^1H NMR (700 MHz, $CDCl_3$, δ ppm): H_5 1.10 (dd, 6H, J_{H-H} = 6.93 Hz); H_1 1.72 (s, 3H); H_{10} 2.14 (s, 3H); H_7 2.23 (s, 18H); H_4 2.23 (sept, 1H); H_2 5.20 (d, 1H, J_{H-H} = 6.02 Hz); $H_{2'}$ 5.44 (d, 1H, J_{H-H} = 5.95 Hz); H_3 5.79 (d, 1H, J_{H-H} = 5.95 Hz); $H_{3'}$ 5.85 (s, 1H); H_6 6.82 (s, 6H); H_8 7.03 (s, 3H); H_{12} 7.05 (t, 1H, J_{H-H} = 6.79 Hz); H_{11} 7.39 (d, 1H, J_{H-H} = 7.63 Hz); H_9 8.52 (s, 1H); H_{13} 8.63 (s, 1H).$^{13}C\{^1H\}$ NMR (176.12 MHz, $CDCl_3$, δ ppm): C_a 17.85; C_g 18.16; C_k 21.08; C_o 22.80; C_f 30.55 (d, J_{C-H} = 3.91 Hz); $C_{c'}$ 86.25; C_c 88.81; C_d 89.14; $C_{d'}$ 92.70; C_b 102.59; C_e 113.72 (d, J_{C-H} = 5.21 Hz); C_q 124.65; C_h 129.42; C_i 131.52; C_j 132.87; C_l 135.73; C_p 138.11; C_n 138.80; C_r 153.36; C_m 156.32.C, H assign confirmed by COSY, HSQC, HMBC (see S.I.) (FTIR, cm^{-1}): 3078 (ν_{asCsp^2-H}), 2972, 2924, 2860 (ν_{asCsp^3-H}), 1593 ($\nu_{asC=N}$), 1473, 1421 ($\nu_{asC=C}$), 1120, 561 (ν_{P-C}), 840 (ν_{PF6^-}), 687 (δ_{C-H}(aromatic ring)). UV-vis (CH_2Cl_2, 1 x 10^{-4} mol L^{-1}) λ max/nm (ε max/L mol^{-1} cm^{-1}): 240 (9200); 276 (6100); 343 (1250); 548 (900).

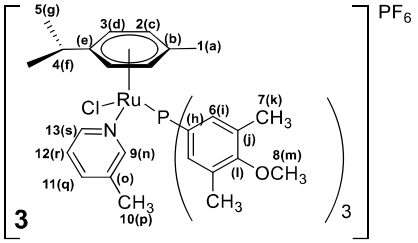

[Ru(η^6-*p*-cymene){P(C$_6$H$_2$-4-MeO-3,5-(Me)$_2$)$_3$}(NC$_5$H$_4$-3-Me)Cl]PF$_6$ (**3**). Yellow solid. Yield: 55.2 mg (86.54 %). MM: 945.22 g·mol^{-1}. M.p.: 152–175 °C (dec). Elemental analysis calc. for: $C_{43}H_{54}ClF_6NO_3P_2Ru$ (%): C, 54.63; H, 5.76; N, 1.48. Found: C, 55.80; H, 5.52; N, 1.49. Λm: 123.4 S cm^2 mol^{-1} (24 h, 25ºC^{31}P{^{1}H} NMR (161.97 MHz, $CDCl_3$, δ ppm): 33.80; -131 to -157 (sept, PF_6). ^{1}H NMR (700 MHz, $CDCl_3$, δ ppm): H_5 1.11 (dd, 6H, J_{H-H} = 6.93 Hz); H_1 1.72 (s, 3H); H_{10} 2.17 (s, 3H); H_7 2.24 (s, 18H); H_4 2.24 (sept, 1H); H_8 3.73 (s, 9H); H_2 5.20 (d, 1H, J_{H-H} = 6.02 Hz); $H_{2'}$ 5.44 (d, 1H, J_{H-H} = 6.02 Hz); H_3 5.79 (d, 1H, J_{H-H} = 6.02 Hz); $H_{3'}$ 5.85 (d, 1H, J_{H-H} = 6.09 Hz); H_6 6.85 (s, 6H); H_{12} 7.07 (t, 1H, J_{H-H} = 6.58 Hz); H_{11} 7.40 (d, 1H, J_{H-H} = 7.63 Hz); H_9 8.54 (s, 1H); H_{13} 8.61 (s, 1H).^{13}C{^{1}H} NMR (176.12 MHz, $CDCl_3$, δ ppm): C_k 16.32; C_a 17.94; C_g 21.00; C_p 22.84; C_f 30.55; C_m 59.74 (d, J_{C-H} = 14.70 Hz); $C_{c'}$ 86.01; C_c 88.70; C_d 88.94; $C_{d'}$ 92.79; C_b 102.53; C_e 113.86 (d, J_{C-H} = 5.91 Hz); C_r 124.70; C_i 131.38; C_j 134.37; C_o 135.66; C_q 138.66; C_n 153.52; C_s 156.38; C_l 159.21. C, H assign confirmed by COSY, HSQC, HMBC (see S.I.) (FTIR, cm^{-1}): 3072 ($\nu_{asCsp^2\text{-}H}$), 2932, 2864, 2827 ($\nu_{asCsp^3\text{-}H}$), 1586 ($\nu_{asC=N}$), 1480, 1426 ($\nu_{asC=C}$), 1112, 552 ($\nu_{P\text{-}C}$), 840 (ν_{PF6^-}). UV-vis (CH_2Cl_2, 1 x 10^{-4} mol L^{-1}) λ max/nm (ε max/L mol^{-1} cm^{-1}): 244 (11100); 276 (6600); 335 (1300); 544 (790).

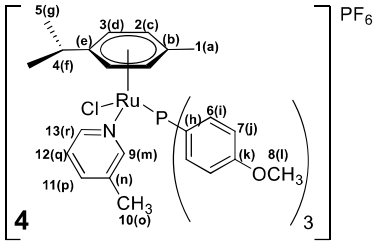

[Ru(η^6-*p*-cymene){P(C$_6$H$_4$-4-MeO)$_3$}(NC$_5$H$_4$-3-Me)Cl]PF$_6$ (**4**). Yellow solid. Yield: 41.0 mg (70.80 %). MM: 861.13 g·mol^{-1}. M.p.: 140–170 ºC (dec). Elemental analysis calc. for: $C_{37}H_{42}ClF_6NO_3P_2Ru$ (%): C, 51.60; H, 4.92; N, 1.63. Found: C, 52.45; H, 4.85; N, 1.76. Λm: 140.0 S cm^2 mol^{-1} (24 h, 25ºC^{31}P{^{1}H} NMR (161.97 MHz, $CDCl_3$, δ ppm): 34.11; -131 to -157 (sept, PF_6). ^{1}H NMR (700 MHz, $CDCl_3$, δ ppm): H_5 1.08 (dd, 6H, J_{H-H} = 7.00 Hz); H_1 1.69 (s, 3H); H_{10} 2.14 (s, 3H); H_4 2.18 (sept, 1H, J_{H-H} = 6.79 Hz); H_8 3.82 (s, 9H); H_2 5.26 (d, 1H, J_{H-H} = 6.02 Hz); $H_{2'}$ 5.46 (d, 1H, J_{H-H} = 5.88 Hz); H_3 5.83 (d, 1H, J_{H-H} = 6.02 Hz); $H_{3'}$ 5.88 (d, 1H, J_{H-H} = 5.95 Hz); H_6 6.87 (s, 6H); H_{12} 7.07 (t, 1H, J_{H-H} = 6.23 Hz); H_7 7.20 (s, 6H); H_{11} 7.38 (d, 1H, J_{H-H} = 7.63 Hz);

H_9 8.51 (s, 1H); H_{13} 8.73 (s, 1H).$^{13}C\{^1H\}$ NMR (176.12 MHz, $CDCl_3$, δ ppm): C_a 18.12; C_g 21.04; C_o 22.96; C_f 30.75; C_l 55.42 (d, J_{C-H} = 18.02 Hz); $C_{c'}$ 84.44; C_c 88.68; $C_{d'}$ 89.19; C_d 94.05; C_b 103.05; C_e 114.01 (d, J_{C-H} = 6.94 Hz); C_h 120.98; C_q 125.03; C_i 135.60; C_j 135.83; C_n 135.83; C_p 138.72; C_r 153.60; C_m 156.29; C_k 161.61. C, H assign confirmed by COSY, HSQC, HMBC (see S.I.) (FTIR, cm^{-1}): (cm^{-1}): 3076 (ν_{asCsp^2-H}), 2968, 2839 (ν_{asCsp^3-H}), 1580 ($\nu_{asC=N}$), 1491, 1453 ($\nu_{asC=C}$), 1100, 557 (ν_{P-C}), 841 (ν_{PF6^-}). UV-vis (CH_2Cl_2, 1 x 10^{-4} mol L^{-1}) λ max/nm (ε max/L mol^{-1} cm^{-1}): 239 (11300); 277 (7330); 551 (710).

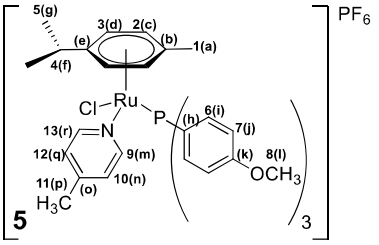

[Ru(η^6-*p*-cymene){P(C$_6$H$_4$-4-MeO)$_3$}(NC$_5$H$_4$-4-Me)Cl]PF$_6$ (5). Orange solid. Yield: 52.7 mg (91.2 %). MM: 861.13 g·mol^{-1}Λm: 137.0 S cm^2 mol^{-1} (24 h, 25ºC). Elemental analysis calc. for: $C_{37}H_{42}ClF_6NO_3P_2Ru$ (%): C, 51.28; H, 4.89; N, 1.62. Found: C, 51.18; H, 4.59; N, 1.83. $^{31}P\{^1H\}$ NMR (121.51 MHz, $CDCl_3$, δ ppm): 33.72; -135 to -153 (sept, PF_6). ^1H NMR (300 MHz, $CDCl_3$, δ ppm): H_5 1.09 (dd, 6H, J_{H-H} = 6.90 Hz); H_1 1.68 (s, 3H); H_4 2.19 (sept, 1H, J_{H-H} = 7.29 Hz); H_{11} 2.28 (s, 3H); H_8 3.82 (s, 9H); H_2 5.22 (d, 1H, J_{H-H} = 6.21 Hz); $H_{2'}$ 5.40 (d, 1H, J_{H-H} = 5.52 Hz); H_3 5.83 (d, 1H, J_{H-H} = 6.45 Hz); $H_{3'}$ 5.87 (d, 1H, J_{H-H} = 6.42 Hz); H_6 6.87 (s, 6H); H_{12} 6.94 (t, 1H, J_{H-H} = 6.18 Hz); H_7 7.19 (s, 6H); H_{10} 7.19 (s, 1H); H_9 8.63 (s, 1H); H_{13} 8.65 (s, 1H).$^{13}C\{^1H\}$ NMR (176.12 MHz, $CDCl_3$, δ ppm): C_a 22.36; C_g 25.62; C_p 31.27; C_f 35.05; C_l 67.99 (d, J_{C-H} = 15.88 Hz); $C_{c'}$ 83.90; C_c 87.76; $C_{d'}$ 90.62; C_d 93.05; C_b 102.93; C_e 114.84; C_q 124.83; C_i 126.78; C_j 128.38; C_n 128.38; C_o 130.30; C_r 150.71; C_m 150.71; C_k 155.20. (FTIR, cm^{-1}): 3080 ($\nu_{as}Csp_2$ -H), 2960 e 2831 ($\nu_{as}Csp_3$-H), 1595(ν_{as}C=N), 1467,1440(ν_{as}C=C), 1117(νP-C), 1258(νC-H), 837(δC-H(aromatic)). UV-vis (CH_2Cl_2, 1 x 10^{-4} mol L^{-1}) λ max/nm (ε max/L mol^{-1} cm^{-1}): 276 (9340), 343 (1328).

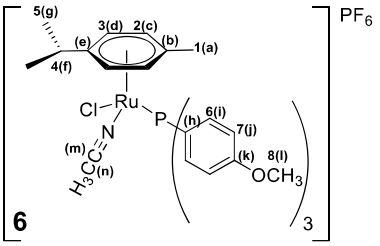

[Ru(η^6-*p*-cymene){P(C$_6$H$_4$-4-MeO)$_3$}(NCCH$_3$)Cl][PF$_6$] (6) Yellow solid. Yield: 37.0 mg (74 %). MM: 808.09 g·mol^{-1}. Elemental analysis calc. for: $C_{33}H_{38}ClF_6NO_3P_2Ru.CH_2Cl_2$(%): C, 45,68; H, 4,51; N, 1,57. Found: C, 46,13; H, 4,35; N, 1,67. P.F.: 214°C. P.D.: 224°C Λm: 155.2 S cm^2 mol^{-1} (24 h, 25ºC). $^{31}P\{^1H\}$ NMR (161.97 MHz, $CDCl_3$, δ ppm): 32.25; -135 to -153 (sept, PF_6). ^1H NMR (400 MHz, $CDCl_3$, δ ppm): H_5 1.36 (dd, 6H, J_{H-H} = 7.40 Hz); H_1 1.75 (s, 3H); H_8 2.00 (s, 3H); H_4 3.04 (sept, 1H, J_{H-H} = 4.60 Hz); H_9 3.85 (s, 9H); H_2 4.60 (d, 1H, J_{H-H} = 6.61 Hz); $H_{2'}$ 5.30 (d, 1H, J_{H-H} = 5.92 Hz); H_3 5.89 (d, 1H, J_{H-H} = 6.55 Hz); $H_{3'}$ 6.11 (d, 1H, J_{H-H} = 6.09 Hz); H_6 6.99 (d, 6H, J_{H-H} = 8.53 Hz); H_7 7.49 (t, 1H, J_{H-H} = 9.00 Hz). $^{13}C\{^1H\}$ NMR (100.61 MHz, $CDCl_3$, δ ppm): C_a 18.39; C_g 21.14; C_n 23.53; C_f 31.27; C_l 55.45; $C_{c'}$ 84.26; C_c 88.69; $C_{d'}$ 89.49; C_d 95.63; C_b 103.38; C_e 114.22 (d, J_{CH} = 11.58 Hz); C_h 121.40 (d, J_{CH} = 55.25 Hz); C_m 127.20; C_i 135.97; C_j 136.01; C_k 161.84. FTIR (cm^{-1}): 3070 ($\nu_{asCsp^2\text{-}H}$), 2972, 2939 e 2841 ($\nu_{asCsp^3\text{-}H}$), 1591, 1499 e 1458 ($\nu_{as\ C=C}$), 1021, 1254 ($\nu_{asC\text{-}O}$), 1096, 557 ($\nu_{P\text{-}C}$), 840 (ν_{PF6^-}). UV-vis (CH_3CN, 1 x 10^{-4} mol L^{-1}) λ max/nm (ε max/L mol^{-1} cm^{-1}): 336 (2266), 433 (372).

X-ray Crystallography

Suitable crystals were grown as per the bulk recrystallization described above. SC-XRD was undertaken using Cu K_α (λ = 1.54184 Å) and Mo K_α (λ = 0.71073) radiation at 100 K on a Rigaku-Oxford Diffraction SuperNova diffractometer equipped with a Pilatus P200 HPC detector. All data collection, integration and intensity corrections were undertaken using CrysAllisPro 1.171.38.41 (Rigaku Oxford Diffraction, 2015). The reported structures for **1–4** and **6** are from Cu and **5** from the Mo datasets (Table 1). Structure determination with the bulky ligands **L1** and **L2** were characteristically challenging [34]. For both **1** and **2**·$CHCl_3$, *Z*' = 2, wherein the two independent cations differ in small details of ligand substituent orientation. In **1** the second cation has a rotationally disordered 3-picoline ligand, so all discussion is of the first, ordered, structure. The two cations of **2**·$CHCl_3$ are both fully ordered (as also are the PF_6^- counter ion and $CHCl_3$ solvate) and their geometries are highly similar and can be averaged. The structure of **3** was extremely challenging and was ultimately modelled successfully as a whole molecule disorder; the geometry is reported for the major component. Structures **4–6** are straightforward. All the final structure models are of good to excellent quality. Full details of the structure solution and refinement are provided in the SI. Structure solution employed SHELXT [43], and refinement SHELXL [44] within OLEX2 [45] Final data analysis and structure visualization was undertaken with Mercury CSD 4.0.0 [46].

Table 1. Crystal data and structure refinement details for structures **1– 6**.

Parameter	**1**	**2**·$CHCl_3$	**3**	**4**	**5**	**6**
Chemical Formula	$C_{58}H_{84}ClF_6NP_2Ru$	$C_{41}H_{49}Cl_4F_6NP_2Ru$	$C_{43}H_{54}ClF_6NO_3P_2Ru$	$C_{37}H_{42}ClF_6NO_3P_2Ru$	$C_{37}H_{42}ClF_6NO_3P_2Ru$	$C_{33}H_{38}ClF_6NO_3P_2Ru$
Formula Weight (g/mol)	1107.72	974.62	945.33	861.17	861.17	809.10
Temperature (K)	100.0(3)	116.2(7)	116.1(3)	99.97(16)	116.6(5)	116.6(4)
Crystal System	Monoclinic	triclinic	Monoclinic	Triclinic	triclinic	Triclinic
Space Group	$P2_1/c$	$P\bar{1}$	$P2_1/c$	$P\bar{1}$	$P\bar{1}$	$P\bar{1}$
A (Å)	15.49034(13)	15.7484(3)	19.4757(2)	11.2877(2)	11.3528(3)	9.6220(2)
b (Å)	19.01025(14)	16.5043(3)	12.25610(10)	11.4003(3)	11.5201(3)	10.2967(2)
c (Å)	39.7747(5)	16.7772(3)	18.8437(2)	16.5321(4)	16.1773(4)	17.8674(4)
α (°)	90	79.2390(10)	90	84.037(2)	73.709(3)	80.072(2)
β (°)	92.6841(9)	88.1370(10)	106.7620(10)	76.216(2)	87.918(2)	78.660(2)
γ (°)	90	85.2890(10)	90	62.869(2)	64.440(3)	81.714(2)
Volume ($Å^3$)	11699.81(19)	4268.85(14)	4306.81(8)	1838.76(8)	1823.27(10)	1698.49(6)
Z	8	4	4	2	2	2
Z'	2	2	1	1	1	1
R_{int}	0.0854	0.0544	0.0411	0.0418	0.0522	0.0509
$R_1{}^a$ [I ≥ 2σ(I)]	0.0678	0.0652	0.0397	0.0444	0.0399	0.0555
wR_2 [I ≥ 2σ(I)]	0.1556	0.1886	0.0957	0.1294	0.1095	0.1391
CCDC	2163114	2163115	2163116	2163117	2163118	1894829

Results and discussion

Synthesis and characterization of the complexes

Six novel cationic ruthenium sandwich complexes **1**-**6** were prepared from **P1 – P4** as orange and yellow solids, stable to light and in air, with yields ranging from 67-91 % as shown in Scheme 1. The four phosphines **L1 – L4** differ significantly in lipophilicity in the order **L1** > **L2** > **L3** > **L4**. The donor strengths (basicities) have also been investigated [35], indicating that **L4** > **L3** > **L2** ~ **L1**. Each of these has been paired with 3-methylpyridine as the larger and less symmetric nitrogen donor ligand in a systematic fashion. For comparisons to other nitrogen donors, the most

basic phosphine **L4**, which is also the least sterically hindered, was employed with 4-methylpyrine and with acetonitrile.

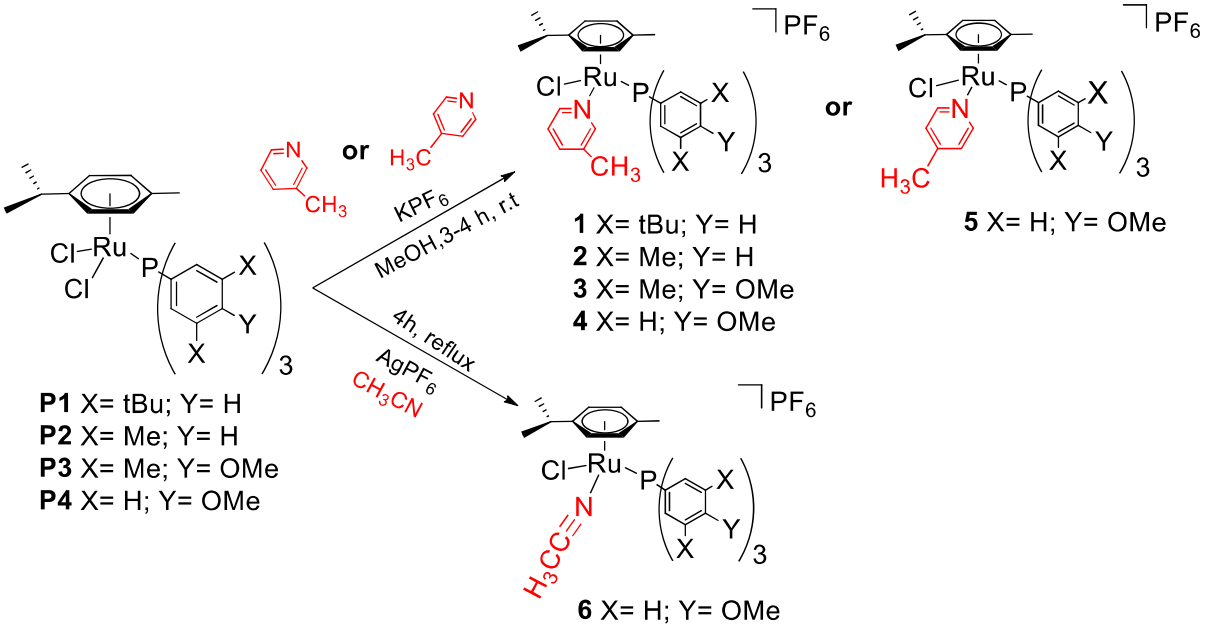

Scheme 1. Synthesis for reactions of cationic complexes **1**-**6**.

These cationic complexes have conductivity (Λ_m) values from 126.1 to 155.2 S cm^2 mol^{-1}. This result provides strong confirmation that these new cationic complexes exist as 1:l electrolytes in solution. Complexes **1**-**6** were bulk recrystallized and were produced in high purity, evidenced by NMR spectra and elemental analysis, which are consistent with the proposed formulae, except that **2** was found to have an EA consistent with the formula **2**·0.5 $CHCl_3$; evidently, some of the solvent of crystallization in **2**·$CHCl_3$ (as confirmed by SC-XRD) had leached out in the time it took to obtain the analysis. All the complexes are soluble in halogenated and polar organic solvents such as DMSO, dichloromethane, acetonitrile, methanol, ethanol, and chloroform but insoluble in water and diethyl ether.

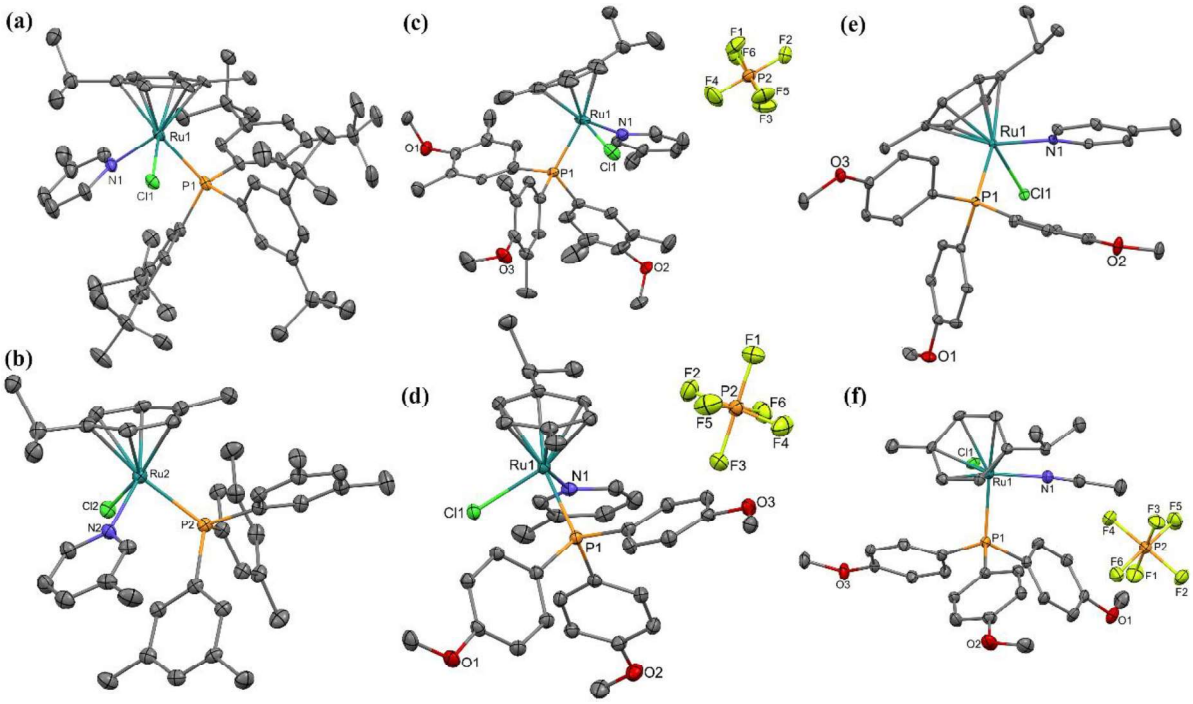

Figure 1. Displacement ellipsoids plots (40% probability) of structures found by crystallography for (a) the ordered cation found in **1**; (b) the second cation in **2**; (c) **3**; (d) **4**; (e) the cation in **5**; (f) **6**. H-atoms on C, the $CHCl_3$, anions and a second cation of **2**·$CHCl_3$, the anions of **1** and **5** and a second cation of **1** are omitted from the views. Only key atom labels are shown, for clarity.

The compositions of **1-6** have been unambiguously confirmed in the solid state by SC-XRD. In the isolated crystals, only **2** was found to be a 1:1 solvate with $CHCl_3$ (see Experimental section and Table 1); all remaining salts crystallized solvent-free. Each structure consists of a unipositive complex cation bearing the phosphine ligands **L1**-**L4** and L^N = 3-methylpyridine, 4-methylpyridine or CH_3CN attached to the organometallic Ru(η^6-*p*-cymene)Cl fragment. The counter-ion is in each case PF_6^-, and in the sole case of **2**·$CHCl_3$, there is also one molecule of solvent in the asymmetric unit. Considering the unit cell volumes in Table 1, calibrating for *Z* and removing the calculated molecular volume of $CHCl_3$ (134 Å^3), gives a volume occupied per formula unit of **1** > **3** > **2** > **4** > **5** > **6**: 1462.5, 1076.7, 933.2, 919.4, 911.6 and 849.2 Å^3. This accurately reflects the decreasing sizes of the phosphines **L1**-**L4**, and a greater occupied volume for 3-methyl- vs. 4-methylpyridine, with CH_3CN having the smallest occupied volume. These data also demonstrate the very large volume of the highly lipophilic **L1** [34-35].

Selected bond lengths for **1-6** are provided in Table 2 and exhaustive measured and derived parameters are provided in the SI, where the full complexity encountered for the structures and important intermolecular contacts are described in detail. The adopted refinement models are all very reliable and key features are described here. The coordination geometries are remarkably uniform for all six complexes, as is especially visible in Fig. 1e showing the cation geometry of compound **5**. The phosphines are all found in a close-to-helical conformation and fill one of three of the piano stool 'legs' of the Ru(η^6-*p*-cymene)X_3 *pseudo*-octahedral geometry; chloro and pyridine ligands complete these sites. The larger ^{i}Pr substituent of the *p*-cymene group is directed away from the phosphine, probably for steric reasons. Noticeably, the 4-methylpyridine group (N1, C41-45) is oriented in such a way as to be parallel to one of the phosphine aryl rings (C21-26). The ring centroid of the pyridine ring is directed over an edge of the phosphine aryl group (C22,23) in an approximation to a typical π-stacking arrangement; a very similar arrangement is encountered in the 3-methylpyridine structures **1-4** (see SI), while even the CH_3CN ligand in **6** is in this general location. Consideration of space-filling models suggests that the conformations adopted are primarily an accommodation to the overall steric demands of the combination of ligands around the metal; evidence that this demand persists in the solution phase is obtained from NMR data (see below).

Table 2. Selected bond distances found in crystal structures of **1-6** and precursors [a,b]

Bond lengths:	Ru-P	Ru-Cl	Ru-N	Ru-C_{cym} (ave)
1	2.3703(11)	2.3892(11)	2.148(4)	2.23(2)
P1	2.366(8)	2.416(4), 2.408(2)		2.215(2)
2	2.3711(11)	2.3999(11)	2.139(4)	2.22(3)
P2	2.426(2)	2.409(10), 2.426(1)		2.23(5)
3	2.3592(17)	2.410(10)	2.116(3)	2.26(7)
P3	2.3824(6)	2.4153(7), 2.4189(6)		2.21(3)
4	2.3674(8)	2.3955(8)	2.146(3)	2.23(3)
P4	2.3693(12)	2.4101(13), 2.4250(11)		2.216(2)
5	2.3740(7)	2.3979(7)	2.131(2)	2.23(3)
6	2.3684(13)	2.3880(12)	2.058(4)	2.23(2)

[a] For **1**, only the first, ordered, of two independent cations are listed; for **2** is the average of the two independent cations; **3** the major component of the whole molecule disorder is listed. [b] Comparison geometries for neutral precursors (**P1-P4**) are from ref. [34], each of which has two Ru–Cl bonds and none to N.

In the metric parameters, the Ru–Cl bond lengths are found to be slightly elongated with the known donor strengths of the phosphines [35], i.e. with **L4** > **L3** > **L2** > **L1**, but the Ru–P bonds seem to get somewhat longer with the increased distal steric bulk of the phosphines. When a comparison is taken between the bonds in cationic **1-6** with those of the neutral precursors **P1-P4,** the Ru–P and Ru–Cl bonds are shortened, on average, by 0.6 and 0.8%, respectively, whereas the average Ru–C_{cymene} lengths are increased by, on average, 0.75%.

The $^{31}P\{^{1}H\}$ NMR spectra (Fig. S1) all show a singlet with chemical shifts in the range 33 – 40 ppm, reflecting the different aryl substituents at P, and a septet at -144 ppm corresponding to the PF_6^- counter-ions. When compared with the chemical shifts of **P1 – P4** (Table 3) [34], the phosphine signals are deshielded, with Δδ ranging from +8.55 to +12.72 ppm. This deshielding accompanies the shortening of the Ru-P bonds in the cationic complexes, indicative of charge depletion at the P nuclei.

Table 3. $^{31}P\{^{1}H\}$-NMR for complexes **1–6**, precursor complexes **P1-P4** and free phosphines **L1-L4**.

[Ru(*p*-cym)(PAr$_3$)Cl$_2$] [a]	**PAr$_3$** [a] δ (ppm)	**Complex** [a] δ (ppm)	**Δδ** [a,b] (ppm)	**[Ru(*p*-cym)(PAr$_3$)L^{N}Cl]$^+$**	**Complex** δ (ppm)	**Δδ** [c] (ppm)	**Δδ** [d] (ppm)
P1	-1.31	+27.20	+28.51	**1**	+39.92	+41.23	+12.72
P2	-2.75	+24.20	+26.95	**2**	+35.86	+38.61	+11.66
P3	-5.55	+22.00	+27.55	**3**	+33.80	+39.35	+11.80
P4	-8.03	+23.70	+31.73	**4**	+34.11	+42.14	+10.41
P4	-8.03	+23.70	+31.73	**5**	+33.72	+41.75	+10.02
P4	-8.03	+23.70	+31.73	**6**	+32.25	+40.18	+8.55

[a] Ref. [34]

[b] $\Delta\delta = \delta_{Precursor\ complex} - \delta_{PAr_3(free)}$

[c] $\Delta\delta = \delta_{Cationic\ complex} - \delta_{PAr_3(free)}$

[d] $\Delta\delta = \delta_{Cationic\ complex} - \delta_{Precursor\ complex}$

The ^{1}H NMR spectra (Fig. S2-S25 and Table S2) show four sets of doublets (H_2, H_3, $H_{2'}$, $H_{3'}$) referring to the four C–H substituents on the η^6-*p*-cymene rings. This feature differs from those of **P1 – P4**, which show only two sets of doublets. The described result is due to the lowered

symmetry of the complexes from replacing one of the chloro ligands by L^N. Additional signals from 7.00 to 8.80 ppm in the spectra of **1 – 5** occur from the aromatic protons of the methylpyridine ligands. The signal in the low frequency regions around 2.13 - 2.24 ppm (H_{10}) for these complexes indicates the presence of the CH_3 group of these L^N [19]. For complex **6** the acetonitrile CH_3 group (H_6) appears at 1.99 ppm. The multiplicity of the H signals in the ^iPr are also altered from doublets in **P1 – P4** to doublets-of-doublets in all these cationic complexes, also reflecting the lower symmetry which induces anisochronous magnetic environments.

The FTIR spectra (Fig. S26-S28 and Table S2) contain the expected bands for the L^N in addition to those of the η^6-*p*-cymene, phosphine and chloride entities. The bands around 1580 - 1595 cm^{-1} ($\nu_{asC=N}$) in **1 – 5** indicate the presence of the aromatic L^N [19,47]. For all complexes, the spectra contain bands of strong intensity, not observed in **P1 – P4**, corresponding to the PF_6^- ions around 840 and 847 cm^{-1} [48,49].

The UV-Vis spectra for complexes **1-4**, (Fig. 2 and Table S3) display shoulders of high intensity in the ultraviolet regions of the spectra centered about 268-276 nm (ε = 7000 - 9340 L mol^{-1} cm^{-1}), correspondent to intra-ligand π–π^* transitions of the triarylphosphine (PAr_3), η^6-*p*-cymene and L^N-ligands. For all complexes, bands in the region λ = 335 - 343 nm (ε = 1300 - 1328 L mol^{-1} cm^{-1}) are assigned to metal-ligand charge transfer (MLTC) transitions from ruthenium to π^* orbitals of the ligands. This was confirmed by TD-DFT computations performed on the model complex $[Ru(\eta^6\text{-}p\text{-cymene})PPh_3L^NCl]^+$. This charge transfer occurs between the HOMO-1/LUMO or HOMO-2 and LUMO/LUMO+1 orbitals, where these three orbitals are mainly dominated by the Ru(t_2g) orbitals and the LUMO by a greater contribution of the π^* orbitals of the Cl^- ligand and a small contribution from the *p*-cymene ligand (HOMO (Ru(*d*)/Cl(2*p*)) → LUMO (π^*)). A region of lower energy observed in the electronic spectra with lower intensity bands, close to λ = 544-551 nm (ε = 790-710 L mol^{-1} cm^{-1}) for the cations in **1 - 4** are attributed to d-d transitions amongst the t_{2g} and e_g MOs of ruthenium. The low molar absorptivity values found for the series complexes also characterize this transition.

For $[Ru(\eta^6\text{-}p\text{-cymene})PPh_3L^NCl]^+$ in **5** with L^N = 4-methylpiridine, the band centered at λ = 276 nm (ε = 9340 L mol^{-1} cm^{-1}) is described as HOMO-1/LUMO or HOMO-2/LUMO majorly

composed by Ru(t_{2g}) atomic orbitals hybridized with Cl(*p*), indicating a π–π* electronic excitation mechanism. Further, the experimental band centered at λ = 343 nm (ε = 1328 L mol^{-1} cm^{-1}) is associated with HOMO/LUMO+1 primary composed by Ru(e_g) with ligand contributions of Cl and *p*-cymene, suggesting an LMCT transition coincident with the *d-d* electronic transition.

Moving to the cation in **6**, with L^N = acetonitrile, the band centered at λ = 336 nm (ε = 2266 L mol^{-1} cm^{-1}) is described as HOMO-1/LUMO major composed by Ru(t_{2g}) atomic orbitals hybridized with Cl(*p*) and PPh_3(*p*), indicating the π–π* electronic excitation mechanism associated with the LMCT. Further, the experimental band centered at λ = 433 nm (ε = 372 L mol^{-1} cm^{-1}) is associated with HOMO-1/LUMO+1 primarily composed of Ru(e_g) with ligand contributions of Cl(*p*) and *p*-cymene(*p*), suggesting an LMCT transition coincident with the *d-d* electronic transition.

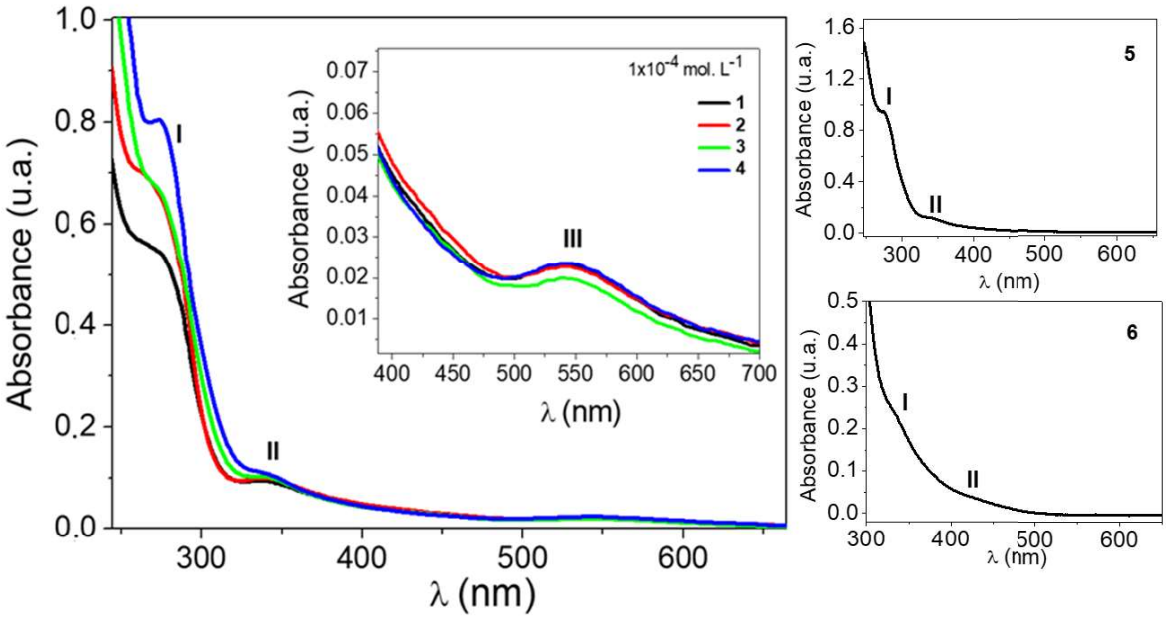

Figure 2: Electronic absorption spectra of **1-6** complexes.

Voltammetric characterization of the complexes

Cyclic voltammetry of cationic complexes **1–6** was performed in order to propose an electrochemical mechanism for these cationic ruthenium(II)-arene complexes. CVs shown in Fig. 3 were recorded in CH_3CN containing 0.1 mol L^{-1} TBAP as supporting electrolyte and using glassy

carbon as working electrode and a Ag/AgCl reference electrode. The cyclic voltammograms of **1**-**6** were recorded from -1.8 to +1.8 V and showed a similarity in the redox profile for all the complexes.

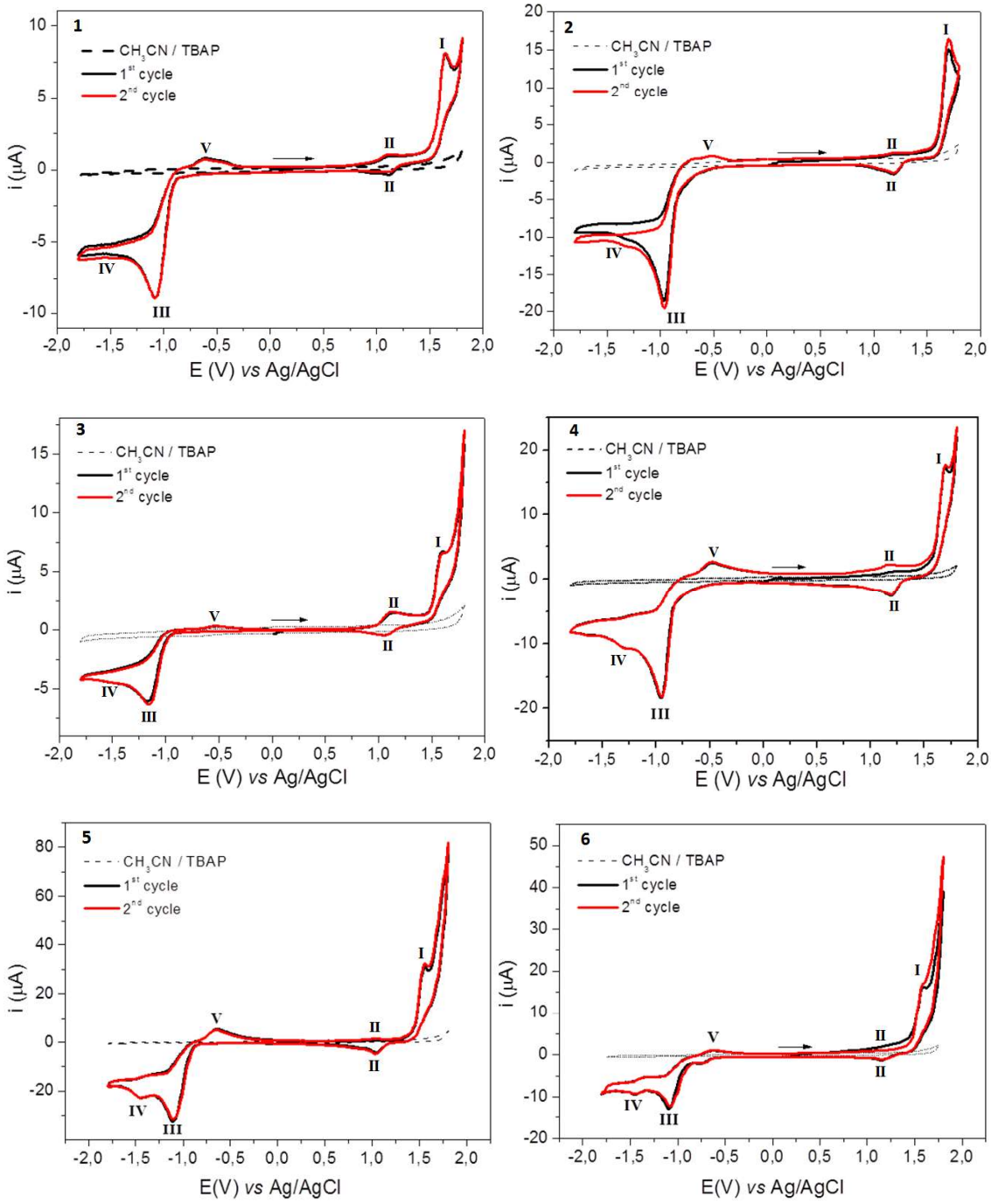

Figure 3. Cyclic voltammograms for complexes **1-6** to 2.0. 10^{-3} mol L^{-1} in TBAP/CH_3CN 0.1 mol L^{-1} vs Ag/AgCl, obtained at 100 mV s^{-1}.

The first oxidation and reduction process are centered at the metal [47,50]. In the first anodic step, an oxidation process occurs at E_{pa}^{I} = +1.55 - +1.67 V, assigned to an independent process of oxidation of $Ru^{(II/III)}$, in according to proposed mechanism (Scheme 2). This process occurs at the same potential range value as to [RuCl(η^6-*p*-cymene)(P-N^R-P)]BF_4 (+1.57 to 1.59 V) [51]. By contrast, this $Ru^{(II/III)}$ couple in the neutral dichloro complexes **P1 – P4** occurs (in CH_3CN) from +1.12 - +1.17 V [52] which is almost identical to the +1.13 - +1.15 V previously published in CH_2Cl_2 [34]. In the latter case, these are close-to-reversible processes, but for **1 - 6**, this Ru oxidation is irreversible at all measured scan rates.

Extrapolating the potential reaching 2.0 V (Fig. S33) an additional oxidation process is detected. This process at ~2.0 V, according to Scheme 1, is attributed to oxidation of the free *p*-cymene after it is dissociated subsequent to process II, as has been independently confirmed by the oxidation of a solution containing pure *p*-cymene [51]. Displacement of the η^6-*p*-cymene in the Ru(III) species is induced by occupation of the three remaining coordination sites by CH_3CN, forming $[Ru(NCCH_3)_3(PAr_3)L^NCl]^{2+}$; this is evidenced by the non-occurrence of such processes in CH_2Cl_2 [34]. These electrochemically created species are reduced at E_{pc}^{II} = +1.04 - +1.16 V *vs*. Ag/AgCl, forming $[Ru(NCCH_3)_3(PAr_3)L^NCl]^+$ (Scheme 2). This is corroborated by electrochemical studies on the chelating diphosphine complex [Ru(η^6-*p*-cymene)(P-NCH_2Ph-P)Cl]$^+$ [51]. When a second scan is recorded on any of **1 – 6**, a new oxidation process with significant smaller current is observed at E_{pa}^{II} = +1.02 - 1.21 V which is attributed to the oxidation $Ru^{(II/III)}$ of species $[Ru(NCCH_3)_3(PAr_3)L^NCl]^+$. To support this argument the first cycle was recorded to show that E_{pa}^{II} does not occur without E_{pa}^{I} (see Fig. S30 in SI). A similar rearrangement was reported upon oxidation of the complex [$RuCl_2(PPh_2(CH_2)_3$-η^6-$C_6H_5)$] where the formation of the new species was confirmed by NMR and SC-XRD from the sample obtained after bulk electrolysis [53]. Estimated values of i_{pa}, i_{pc}, E_{pa} and E_{pc} for all the complexes **1-6** are listed in Table 4.

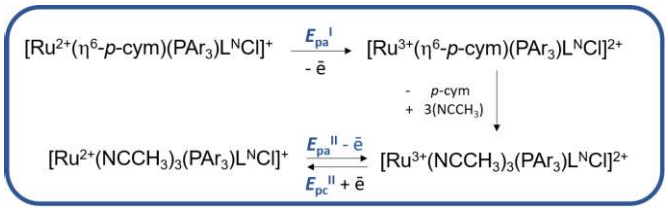

Scheme 2: Representation of the electrochemical and chemical processes for the [Ru(η^6-*p*-cymene)(PAr$_3$)L^{N}Cl][PF$_6$] in the anodic potentials region.

In the cathodic potential region, as proposed in Scheme 3, reduction processes at E_{pc}^{III} = -0.97 to -1.14 V occurs for all six complexes, which is assigned to the Ru$^{(II/I)}$ reduction of the original complexes [Ru(η^6-*p*-cymene)(PAr$_3$)L^{N}Cl]$^+$. That assignment is supported by some cationic Ru(II)-arene complexes ([Ru(η^6-*p*-cymene)(κ^2-O-O-acac)(NCCH$_3$)]$^+$ E_{pc} = -1.24 V [54] and [Ru(η^6-*p*-cymene)(κ^2-O-O-acac)(PMe$_3$)]$^+$ E_{pc} = -1.63 V [54]). Here too, an EC process is postulated with the release of Cl$^-$, resulting in formation of [Ru(η^6-*p*-cymene)(PAr$_3$)(NCCH$_3$)L^N]$^+$. These latter species are then reduced at the very negative potential values (E_{pc}^{IV} = -1.41 to -1.47 V) and oxidized at E_{pa}^{V} = -0.51 to -0.64 V to obtain the [Ru(η^6-*p*-cymene)(PAr$_3$)(NCCH$_3$)L^N]$^{2+}$ complex (Scheme 3).

Finally, quite independently of these mechanistic interpretations, the differences between E_{pa}^{Ia} and E_{pc}^{III} for all complexes **1** - **6** represents a wide redox stability window of ΔE = 2.65 to 3.01 V indicating the high stability of these complexes in the Ru(II) oxidation state afforded by the combined ligand set, a range that is much wider than the physiological E^o range (−1 V to +1 V vs. SHE) [55].

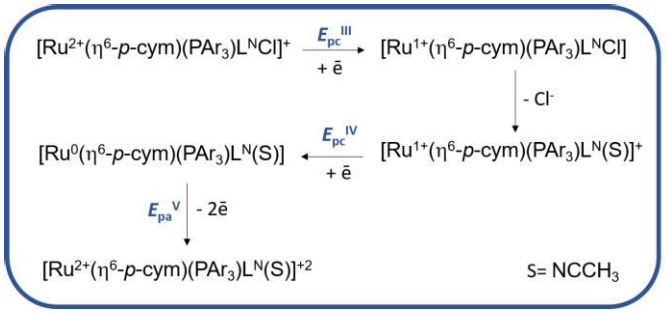

Scheme 3: Representation of the electrochemical and chemical processes for the [Ru(η^6-*p*-cymene)(PAr$_3$)L^{N}Cl][PF$_6$] at cathodic current region.

Table 4.: Values of potentials (V) and peak current i_{pa} and i_{pc} (μA) obtained from cyclic voltammograms of complexes **1-6**.

	E_{pa}^{I}	E_{pa}^{II}	E_{pc}^{II}	$E_{m}^{II\,a}$	i_{pa}/i_{pc}^{II}	$\Delta E_{p}^{II\,b}$	E_{pc}^{III}	E_{pc}^{IV}	E_{pa}^{V}	E_{window} [c]
1	1.64	1.11	1.04	1.07	0.20	0.07	-1.08	-1.47	-0.60	3.11
2	1.67	1.21	1.16	1.18	1.08	0.05	-0.97	-1.43	-0.51	3.10
3	1.61	1.13	1.07	1.10	0.25	0.06	-1.14	-1.46	-0.57	3.07
4	1.65	1.15	1.12	1.13	1.09	0.03	-1.08	-1.41	-0.58	3.06
5	1.55	1.02	1.05	1.03	0.32	0.03	-1.09	-1.45	-0.64	3.00
6	1.58	1.11	1.16	1.14	0.91	0.05	-1.08	-1.43	-0.63	3.01

[a] $E_{1/2}^{II} = (E_{pa}^{II} + E_{pc}^{II})/2$. [b] $\Delta E_{p}^{II} = |E_{pa}^{II} - E_{pc}^{II}|$. [c] $E_{window} = |E_{pa}^{I} - E_{pc}^{VI}|$

From the viewpoint of DFT calculations, the cyclic voltammetry can be interpreted from the analysis of structural fingerprints as a function of the addition or removal of electrons, as reported in Table 5. These results indicate that, when the reduction of the starting Ru(II) complex occurs, the localization of one additional electron in the LUMO orbitals induces an increase in the Ru-Cl bond lengths, which is strongly supportive of the proposed chlorine labilization mechanism, in agreement with the antibonding features of LUMO for all investigated complexes (Fig. S-32).

Table 5.: Bond distances and angles analyzed for $[Ru(\eta^6\text{-}p\text{-cymene})(PPh_3)L^{N}Cl]^{0/+1/+2}$ in different charge states.

N	Bond path	Reduced	Ground State	Oxidized
			Distance (Å)	
3-methylpyridine	Ru-Cl	2.809	2.472	2.348
	Ru-N	2.125	2.162	2.131
	Ru-P	2.639	2.482	2.509
	Ru-C_6	1.721	1.827	1.874
			Angle (°)	
	Cl-Ru-N	90.4	90.2	95.8
	Cl-Ru-P	82.2	84.7	85.8
	N-Ru-P	89.7	88.5	86.7
			Distance (Å)	
4-	Ru-Cl	3.049	2.472	2.348
	Ru-N	2.146	2.166	2.134
	Ru-P	2.483	2.480	2.508
	Ru-C_6	1.821	1.827	1.875

		Angle (°)		
	Cl-Ru-N	89.0	90.4	95.9
	Cl-Ru-P	82.9	84.4	85.8
	N-Ru-P	90.8	88.9	86.9
		Distance (Å)		
	Ru-Cl	4.244	2.453	2.421
	Ru-N	2.061	2.050	2.035
	Ru-P	2.483	2.473	2.512
	Ru-C_6	1.859	1.833	1.880
Acetonitrile		**Angle (°)**		
	Cl-Ru-N	73.9	84.7	85.12
	Cl-Ru-P	86.9	87.7	93.24
	N-Ru-P	90.3	86.2	83.27

The oxidation mechanism was theoretically computed by removing one electron from the HOMO, resulting in an increase in the average Ru-C (*p*-cymene) bond distances, in support of experimental evidence for *p*-cymene displacement by CH_3CN upon oxidation. Furthermore, the Frontier Molecular Orbital (FMO) energies reported in Fig. 4 indicates the electronic role of L^N on the electrochemical properties of $[Ru(\eta^6\text{-}p\text{-cymene})(PPh_3)L^NCl]^+$ complexes in comparison to neutral precursors **P1 – P4** [34]. In this case, the N-based ligands behave as donors resulting in more stabilized HOMO orbitals and higher oxidation potential. On the other hand, the LUMO orbitals are also more negative than neutral precursors [34], suggesting that N-based complexes are harder to reduce. It is also profitable to compare these results for the cationic complexes **1 – 6** with those of the neutral precursors **P1 – P4**, for which the relevant computed model complex $[Ru(\eta^6\text{-}p\text{-cymene})(PPh_3)Cl_2]$ has FMO energies of -4.58 (HOMO) and -2.40 eV. This strongly supports the experimentally observed ~ 0.5 V higher potential for the $Ru^{II/III}$ couple in the cationic complexes **1 – 6**.

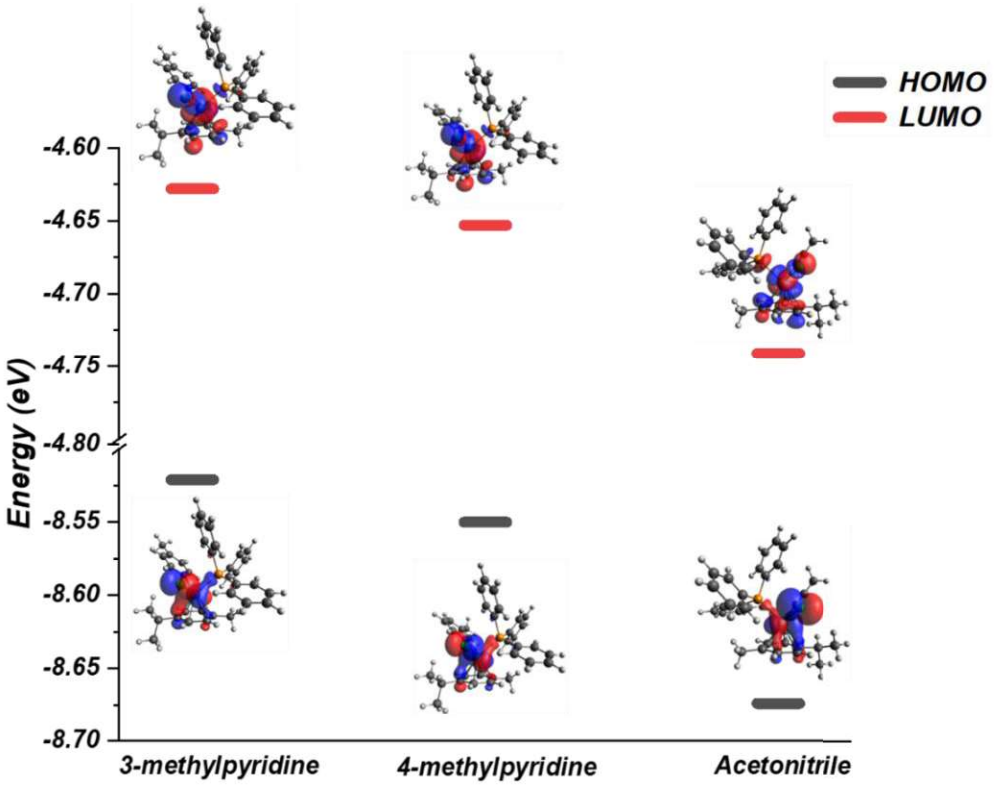

Figure 4. Frontiers molecular orbital energies for [Ru(η^6-*p*-cymene)(PPh_3)L^NCl]$^+$ with N = 3-methylpyridine; 4-methylpyridine; and acetonitrile obtained with the UB3LYP/6-31+G(d)-SPK-DZCD.

Cytotoxicity of ruthenium(II)-arene complexes on human cancer cell lines

Compounds **1**-**6** were evaluated by the MTT cell viability assay. Cells were either treated with dimethylsulfoxide only as solvent control or with a range of concentrations of each compound for 96 hours. The IC_{50} concentrations of compounds **1**-**6** were calculated for U2OS (bone cancer) and HT-29 (colon cancer) cell lines and are shown in Table 6. All compounds demonstrated a moderate toxicity in low micromolar values (μM) for both tested cell lines. Interestingly, the activity was weakest in **5**, which held a 4-methylpyridine substitution. Complexes **1**-**4** and **6** induced a change in cell morphology as noted by the appearance of small vesicles after treatment by 24 h. These vesicles were not observed after treatment with **5** in any of tested concentrations (Fig. 5), which was consistent with the cytotoxicity data.

Table 6.: IC_{50} (μM) values at 96 h for U2OS (bone cancer) and HT-29 (colon cancer) cell lines.

Complexes	U2OS	HT-29

1	4.7	2.8
2	2.5	0.3
3	2.8	1.0
4	3.3	1.5
5	13.9	40.0
6	4.7	0.6

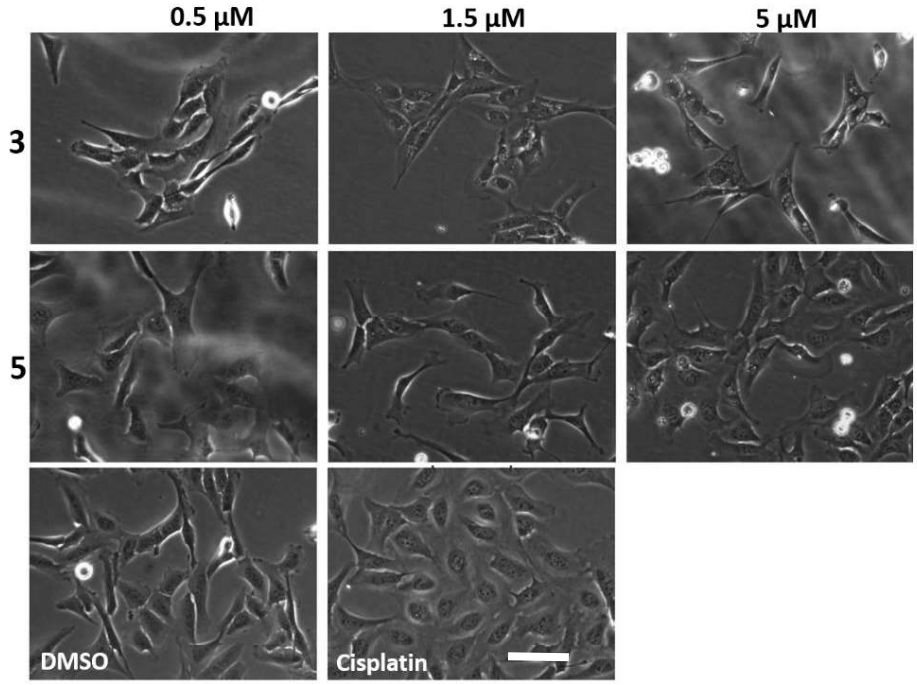

Figure 5.: Phase-contrast light microscopy images defined for **3** and **5** complexes after 24 h. The scale bar represents 50 µm.

For complex **3** at a concentration of 0.5 µM at 24 h the formation of vesicles (small bright spots) is almost imperceptible (Fig. 5). At 1.5 µM, however, vesicles are easier to observe and present in most cells. At 5 µM concentration some cells are dead ceasing cell division (clear rounded dots) and cells have large vesicles. Cells treated with complex **5** show few to no vesicles at any tested concentration and resemble the morphology of the DMSO (vehicle) treated cells. Similar features were presented for complexes (**1**, **4**, **6**) as demonstrated in Fig. S31. In contrast to these results the cells treated with cisplatin do not have vesicles, suggesting that the mechanism of action might be different from that of the complexes tested, confirming the two different mechanisms of action cisplatin described by Swift and Golsteyn which do not include the vesicle

formation [56]. The cytotoxic activity that has been reported for similar neutral and cationic ruthenium-arene complexes in the literature against different cancer cell lines have been compiled and can be found in Table S4 in the Supporting Information.

Conclusions

Six newly synthesized cationic triarylphosphines ruthenium(II)-arene complexes containing methylpyridine (**1-5**) and acetonitrile (**6**) ligands were successfully prepared and characterized. SC-XRD structures were obtained for **1 - 6**, all previously unreported structures. The observed geometry around the ruthenium (II) metal ions in the solid state are all *pseudo*-octahedral. Through electrochemical experiments using cyclic voltammetry, it was observed that the anodic peak potential referring to the $Ru^{II/III}$ oxidation couple occurs at much more positive potentials when compared to the analogous neutral complexes **P1 – P4** due the positive charges at the metal center. It is noteworthy that DFT calculations support the displacement of *p*-cymene upon oxidation to Ru(III), although this is only known to occur in the presence of coordinating solvents such as CH_3CN. Moreover, the fact that both the reduction and oxidation potentials exceed the physiological ΔE range, indicates the large redox stability of cationic ruthenium(II)-arene complexes relative to the *in vivo* biological environment. The biological activity of complexes **1**-**4** and **6** are similar to each other with IC_{50} values in the range of 2.5 to 4.7 μM for U2OS and 0.3 to 2.8 μM for HT-29 cancer cell lines. By contrast, complex **5** was the least active for both tested cell lines. We are in continuous search for cationic ruthenium complexes that would show promising antitumor activities. Our further results from such studies will be reported in due course.

Accession codes

CCDC 1894829 and 2163114-2163118 contain the supplementary crystallographic data for this paper. These data can be obtained free of charge via www.ccdc.cam.ac.uk/data_request/cif , or by emailing data_request@ccdc.cam.ac.uk, or by contacting The Cambridge Crystallographic Data centre, 12 Union Road, Cambridge CB2 1EZ, UK; fax: + 44 1223 336,033.

Acknowledgements

I.D.L.G., F.M. and P.B.R. would like to thank CAPES or CNPq for scholarship. and L.F.B. would like to thank CNPq e Fundação Araucária for scholarship. K.W. acknowledge financial support from the CNPq (432226/2018-4). We are also thankful to the Multi-User Laboratory Complex (C-LabMu/UEPG) for providing the spectroscopy facilities. R.T.B. and R.M.G. thank the NSERC-Canada for ongoing Discovery Grants support. We thank the University of Lethbridge and the Faculty of Arts & Science for purchasing the Super Nova X-ray diffractometer. R.A.P.R. is grateful for the financial assistance from FAPEMIG (project no. APQ-00079-21) and UEMG for the Productivity Program. The authors would also like to thank the National Center for High-Performance Computing (CENAPAD) at UNICAMP and UFC for providing computing resources.

References

[1] S. Ghosh, Bioorg. Chem. 88 (2019) 102925-102945, https://doi.org/10.1016/j.bioorg.2019.102925.

[2] R. Oun, Y.E. Moussa, N.J. Wheate, Dalton Trans. 47 (2018) 6645-6653, https://doi.org/10.1039/C8DT00838H.

[3] R.C. Kiss, F. Xia, S. Aclin, Int. J. Mol. Sci. 22 (2021) 8199, https://doi.org/10.3390/ijms22158199.

[4] S. Parveen, F. Arjmand, S. Tabassum, Eur. J. Med. Chem. 175 (2019) 269-286, https://doi.org/10.1016/j.ejmech.2019.04.062.

[5] J.P.C. Coverdale, T. Laroiya-Mccarron, I. Romero-Canelón, Inorganics. 7 (2019) 31-46, https://doi.org/10.3390/inorganics7030031.

[6] Q. Sun, Y. Li, H. Shi, Y. Wang, J. Zhang, Q. Zhang, Molecules. 26 (2021) 4389, https://doi.org/10.3390/molecules26154389.

[7] S.Y. Lee, C.Y. Kim, T-G. Nam, Drug Des Devel Ther. 14 (2020) 5375, https://doi.org/10.2147/DDDT.S275007.

[8] C. Sonkar, S. Sarkar, S. Mukhopadhyay, RSC Med. Chem. 13 (2022) 22-38, https://doi.org/10.1039/D1MD00220A.

[9] P. Kumar, R.K. Gupta, D.S. Pandey, Chem. Soc. Rev. 43 (2014) 707–733, https://doi.org/10.1039/C3CS60189G.

[10] H.Y. Khan, S.K. Maurya, H.R. Siddique, S. Yousuf, F. Arjmand, ACS Omega. 5 (2020) 15218-15228, https://doi.org/10.1021/acsomega.0c01206.

[11] M.J. Chow, W.H. Ang, in: K.K.-W. Lo (Ed.), Inorganic and organometallic transition metal complexes with biological molecules and living cells, Academic Press, United Kingdom, 2016, pp. 119-146, https://doi.org/10.1016/B978-0-12-803814-7.00004-6.

[12] L. Zheng, C. Yuan, J. Shu, J. Qian, Q. Wu, Y. Chen, R. Wu, X. Ouyang, Y. Li, W. Mei, Molecules. 27 (2022) 1897-1915, https://doi.org/10.3390/molecules27061897.

[13] A. Savića, N. Gligorijević, S. Aranđelović, B. Dojčinović, A.M. Kaczmarek, S. Radulović, R.V. Deun, K.V. Hecke, J. Inorg. Biochem. 202 (2020) 110869-110882, https://doi.org/10.1016/j.jinorgbio.2019.110869.

[14] A.A. Nazarov, C.G. Hartinger, P.J. Dyson, J. Organomet. Chem. 751 (2014) 251-260, https://doi.org/10.1016/j.jorganchem.2013.09.016.

[15] S. Swaminathan, J. Haribabu, N. Balakrishnan, P. Vasanthakumar, R. Karvembu, Coord. Chem. Rev. 459 (2022) 214403-214435, https://doi.org/10.1016/j.ccr.2021.214403.

[16] M.P. Mitoraj, A. Michalak, Inorg. Chem. 49 (2010) 578–582, https://doi:10.1021/ic901736n.

[17] H. Dossmann, D. Gatineau, H. Clavier, A. Memboeuf, D. Lesage, Y. Gimbert, J. Phys. Chem. A 124 (2020) 8753–8765, https://doi:10.1021/acs.jpca.0c06746.

[18] T. Dastan, U.M. Kocyigit, S.D. Dastan, P.C. Kilickaya, P. Taslimi, O. Cevik, M. Koparir, C. Orek, I. Gulçin, A. Cetin, J. Biochem. Mol. Toxicol. 31 (2017) e21971-e21983, https://doi.org/10.1002/jbt.21971.

[19] R. Sáez, J. Lorenzo, M.J. Prieto, M. Font-Bardia, T. Calvet, N. Omeñaca, M. Vilaseca, V. Moreno, J. Inorg. Biochem. 136 (2014) 1-12, https://doi.org/10.1016/j.jinorgbio.2014.03.002.

[20] L. Shadap, J.L. Tyagi, K.M. Poluri, S. Novikov, C-W. T. Lo, Y. Mozharivskyj, M.R. Kollipara, Transit. Met. Chem. 46 (2021) 231-240, https://doi.org/10.1007/s11243-020-00439-z.

[21] Pragti, B.K. Kundu, C. Sonkar, R. Ganguly, S. Mukhopadhyay, Polyhedron. 207 (2021) 115379-, https://doi.org/10.1016/j.poly.2021.115379.

[22] S. Parveen, M. Hanif, S. Movassaghi, M.P. Sullivan, M. Kubanik, M.A. Shaheen, T. Söhnel, S.M.F. Jamieson, C.G. Hartinger, Eur. J. Inorg. Chem. 2017 (2017), 1721-1727, https://doi.org/10.1002/ejic.201601163.

[23] L. Colina-Vegas, K. Oliveira, B. Cunha, M. Cominetti, M. Navarro, A.A. Batista, Inorganics. 6 (2018) 132, https://doi.org/10.3390/inorganics6040132.

[24] Pragti, B.K. Kundu, S. Mukhopadhyay, Coord. Chem. Rev. 448 (2021) 214169-214209. https://doi.org/10.1016/j.ccr.2021.214169.

[25] T. Pieper, W. Peti, B. K. Keppler, Met Based Drugs. 7 (2000) 225-232, https://doi.org/10.1155/MBD.2000.225

[26] V. Vidimar, X. Meng, M. Klajner, C. Licona, L. Fetzer, S. Harlepp, S., P. Hébraud, M. Sidhoum, C. Sirlin, J-P. Loeffler, G. Mellitzer, G. Sava, M. Pfeffer, C. Gaiddon, Biochem. Pharmacol. 84 (2012) 1428–1436, https://doi.org/10.1016/j.bcp.2012.08.022.

[27] L. Belsa, C. López, A. González, M. Font-Bardía, T. Calvet, C. Calvis, R. Messeguer, Organometallics, 32 (2013) 7264–7267, https://doi.org/10.1021/om400941b.

[28] A. Guerriero, W. Oberhauser, T. Riedel, M. Peruzzini, P.J. Dyson, L. Gonsalvi, Inorg. Chem. 56 (2017) 5514–5518, https://doi.org/10.1021/acs.inorgchem.7b00915.

[29] A. Mondal, R.K. Tripathy, P. Dutta, M.K. Santra, A.A. Isab, C.W. Bielawski, H.K. Kisan, S.K. Chandra, J. Dinda, Appl. Organomet. Chem. 33 (2018) e4692-e4706, https://doi.org/10.1002/aoc.4692.

[30] J.A. Gillespie, D.L. Dodds, P.C. Kamer, Dalton Trans. 39 (2010) 2751-2764, https://doi.org/10.1039/B913778E.

[31] L. Biancalana, A. Pratesi, F. Chiellini, S. Zacchini, T. Funaioli, C. Gabbiani, F. Marchetti, New J. Chem. 41 (2017) 14574-14588, https://doi.org/10.1039/C7NJ02300F.

[32] L. Biancalana, L.K. Batchelor, A. de Palo, S. Zacchini, G. Pampaloni, P.J. Dyson, F. Marchetti, Dalton Trans. 46 (2017) 12001-12004, https://doi.org/10.1039/C7DT02062G.

[33] A.L. Noffke, A. Habtemariam, A.M. Pizarro, P.J. Sadler, Chem. Comm. 48 (2012) 5219, https://doi.org/10.1039/C2CC30678F.

[34] I.D.L. Guimarães, F. Marszaukowski, R. Ribeiro, S.R. de Lazaro, K.M. de Oliveira, A.A. Batista, P. Castellen, E. Wrobel, J.R. Garcia, R.T. Boeré, K. Wohnrath, J. Organomet. Chem. 931 (2021) 121599-121638, https://doi.org/10.1016/j.jorganchem.2020.121599.

[35] I.D.L. Guimarães, J.R. Garcia, K. Wohnrath, R.T. Boeré, Eur. J. Inorg. Chem. 32 (2018) 3606-3614, https://doi.org/10.1002/ejic.201800656.

[36] F. Marszaukowski, R.T. Boeré, K. Wohnrath, Cryst. Growth Des. 22 (2022) 2512-2533, https://doi.org/10.1021/acs.cgd.2c00020.

[37] D.D. Perrin, W.L.F. Armarego. Purification of Laboratory Chemicals. 4ª ed., Butterworth Heinemann Press: Oxford., United Kingdom, 1996.

[38] W.J. Geary, Coordination Chemistry Reviews. 7 (1971) 81-122, https://doi.org/10.1016/S0010-8545(00)80009-0.

[39] A.D. Becke, Phys. Rev. A. 38 (1988) 3098-3100, https://doi.org/10.1103/PhysRevA.38.3098.

[40] C. Lee, C.W. Yang, R.G. Parr, Phys. Rev. B. 37 (1988) 785-789, https://doi.org/10.1103/PhysRevB.37.785.

[41] Frisch, M.J., et al., *Gaussian 09 Revision A.2*. 2009.

[42] T. Lu, F. Chen, J. Comput. Chem. 33 (2012) 580-592, https://doi.org/10.1002/jcc.22885.

[43] G.M. Sheldrick, Acta Cryst. Sect. A 71 (2015) 3–8, https://doi.org/10.1107/S2053273314026370.

[44] G.M. Sheldrick, Acta Cryst. Sect. C. 71 (2015) 3–8, https://doi.org/10.1107/S2053229614024218.

[45] O.V. Dolomanov, L.J. Bourhis, R.J. Gildea, J.A.K. Howard, J. Puschmann H., Appl. Crystallogr. 42 (2009) 339–341, https://doi.org/10.1107/S0021889808042726.

[46] C.F. Macrae, I.J. Bruno, J.A. Chisholm, P.R. Edgington, P. McCabe, E. Pidcock, L. Rodriguez-Monge, R. Taylor, J. van de Streek, P. A. Wood, J. Appl. Crystallogr. 41 (2008) 466–470, https://doi.org/10.1107/S0021889807067908.

[47] F. Marchetti, C. Pettinari, A. Cerquetella, A Cingolani, R. Pettinari, M. Monari, R. Wanke, M.L. Kuznetsov, A.J.L. Pombeiro, Inorg. Chem. 48 (2009) 6096-6108, https://doi.org/10.1021/ic900463b.

[48] S.D. Dwivedi, A. K. Singh, S. K. Singh, S. Sharma, M. Chandra, D. S. Pandey, Eur. J. Inorg. Chem. 36 (2008) 5666-5673, https://doi.org/10.1002/ejic.200800867.

[49] P.W. Hansen, P.W. Jensen, Spectrochim. Acta A Mol. Biomol. Spectrosc. 50 (1994) 169-183, https://doi.org/10.1016/0584-8539(94)80125-8.

[50] B.D. Credico, F.F. de Biani, L. Gonsalvi, A. Guerri, A. Ienco, F. Laschi, M. Peruzzini, G. Reginato, A. Rossin, P. Zanello, Chem. Eur. J. 15 (2009) 11985–11998, https://doi.org/10.1002/chem.200901642.

[51] J.P. da Silva, O. Fuganti, M.G. Kramer, G. Facchin, L.E.A. Nascimento, J. Ellena, D.F. Back, A.C.S. Gondim, E.H.S. Silva, L.G.F. Lopes, S. Machado, I.D.L. Guimarães, K. Wohnrath, M.P. de Araujo, Dalton Trans. 49 (2020) 16498-16514, https://doi.org/10.1039/d0dt02500c.

[52] I.D.L. Guimarães and K. Wohnrath, Unpublished results.

[53] P.D. Smith, A.H. Wright, J. Organomet. Chem. 559 (1998) 141-147, https://doi.org/10.1016/S0022-328X(97)00750-X.

[54] T. Sumiyoshi, T.B. Gunnoe, J.L. Petersen, P.D. Boyle, Inorganica Chim. Acta. 361 (2008) 3254–3262, http://doi.org/10.1016/j.ica.2007.10.012.

[55] P. Hosseinzadeh, Y. Lu, Biochim. Biophys. Acta (BBA)-Bioenergetics. 1857 (2016) 557-581, https://doi.org/10.1016/j.bbabio.2015.08.006.

[56] L.H. Swift, R. M. Golsteyn, Biol. Cell. 108 (2016) 127–148, http://doi.org/10.1111/boc.201500056.